VIBRATION OF ROLLER CHAIN DRIVES AT LOW, MEDIUM AND HIGH OPERATING SPEEDS

W. Choi and G. E. Johnson
Design Laboratory
Mechanical Engineering and Applied Mechanics
The University of Michigan
Ann Arbor, MI 48109-2125

enqm

UMR1130

VIBRATION OF ROLLER CHAIN DRIVES AT LOW, MEDIUM AND HIGH OPERATING SPEEDS

W. Choi and G. E. Johnson
Design Laboratory
Mechanical Engineering and Applied Mechanics
The University of Michigan
Ann Arbor, MI 48109-2125
Glen_E._Johnson@um.cc.umich.edu

Abstract

A model based on axially moving material is developed to study transverse vibration in roller chain drives. A unique feature of the work presented in this study is that impact, polygonal action and external periodic load have been included through chain tension and boundary conditions and periodic length change is also considered. The impact between the engaging roller and sprocket surface is modeled as a single impact between two elastic bodies and the modeling of the polygonal action is based on a four bar mechanism (rigid four bar at low speeds, elastic four bar at moderate and high speeds). At low and medium operating speeds, the system equation of motion for the chain span is expressed as a mixed type partial differential equation with time-dependent coefficients and time-dependent boundary conditions. At high operating speeds, the system equations of motion are two partial differential equations for transverse and longitudinal vibrations respectively and they are nonlinearly coupled. The effects on transverse vibration of center distance, the moment of inertia for the driven sprocket system, static tension, and external periodic load are presented and discussed. Solutions are obtained by a finite difference method and Galerkin's method.

Nomenclature

c : chain span velocity

c_i : contact damping coefficient in impact

I_2 : moment of inertia of driven sprocket

k_i : contact stiffness coefficient in impact

L : chain span length

L_0 : the shorter of the two possible span lengths

L_{ct} : length of the common tangent

m_i : effective mass in impact

m_l : mass per unit length of chain

n_1, n_2 : driving and driven sprocket tooth numbers

p_c: chain pitch

r_1, r_2 : radius of driving and driven sprockets

r_t : radius of roller

T_{ex} : magnitude of external periodic loading

T_s : static tension

V_{rel} : relative velocity of a roller to sprocket surface

x_0 : relative displacement of roller to sprocket tooth surface after contact

α_f: phase shift between engagement and disengagement

η : angle between relative velocity of roller and the sprocket surface

λ : pulley support constant

θ : tensioner arm angle

θ_0 : initial tensioner arm angle

ω_1 : angular velocity of driving sprocket

ω_2 : angular velocity of driven sprocket

ω_{ex} : frequency of external periodic loading

1. INTRODUCTION

Chain drives are characterized by the discrete nature of the chain links and sprocket teeth. Compared to belt drives, this discrete nature makes the chain drive unique and gives both advantages and disadvantages. The advantages include no-slip between the chain and the sprocket and lower loads on the shaft bearings. The disadvantages include noise and vibration [1]. These undesirable characteristics have motivated several researchers to investigate the behavior of chain drives including their transverse vibration.

The transverse vibration of a chain strand can be excited by both internal and external stimuli. Periodic torsional loading [2] and imbalance in the drive are external sources; polygonal action and roller-tooth impacts are internal sources. Polygonal action occurs due to the fact that the chain, lying on the sprocket, forms a polygon rather a circle. This chordal nature leads to a fluctuating motion. Previous studies include the effects of center distance and sprocket-tooth numbers on the fluctuation of the velocity ratio of two sprockets [3-5] and the derivation of the dynamic load due to polygonal action [6, 7]. Another internal source corresponds to the impact between the engaging roller and the driving sprocket and it is due to the velocity of the roller relative to the sprocket surface as the roller seats. Research on the impact has been done on the effective mass [8-10], the contact stiffness [11] , the elastic collision [12], and the intensity of impact interacting with transverse vibration [13]. Also the impact force was measured experimentally in [14-16].

Studies of the transverse vibration of the chain have been based on both continuous and discrete models. One type of discrete model encompasses a string loaded with lumped masses [17-19]. An alternate discrete model is based on a series of links [10, 12, 20]. The continuous model is typically based on a uniform string. Transverse vibration and stability analysis of a uniform string was addressed in [21, 22]. Another continuous model that has been applied to study chain drives is the axially moving string. A recent study investigated the stability of an axially moving string subject to the dynamic load due to polygonal action [23]. The discrete model is best suited for the investigation of the detailed dynamics of a chain drive (like the contact mechanics), but it is less well suited for the study of the vibration of a general chain drive (including more than two sprockets) due to the complexity of modeling.

Thus a primary goal of this research is to extend the continuous model to include the dynamic load due to polygonal action, the dynamic load due to impact, and the transverse displacement excitations at the end points of the chain span. The new model will be used to

study the performance (including transverse vibration) of chain drives at low, medium, and high operating speeds.

2. TRANSVERSE VIBRATION IN ROLLER CHAIN DRIVE

2.1 Dynamic Load

2.1.1 Speed Tensioning, Impact, and External Periodic Load

The dynamic loads in roller chain drives are due to speed tensioning, polygonal action, impact and external loading. The dynamic load due to speed tensioning is expressed for a general axially moving material as follows.

$$D_c = \lambda m_1 c^2 \tag{2-1}$$

The value of λ represents the relative stiffness of an axially moving material compared to that of the supporting structure. For a system with one chain span and two sprockets, λ can ranges from 0 to 1 [24]. When λ is one, it means that the axially moving material is very stiff compared to the structure. In the case of roller chain drives, λ is closer to one than to zero for most cases because of the high stiffness of the chain span.

The dynamic load due to impact depends on the effective mass taking part in the impact, the relative impact velocity, roller-tooth contact stiffness and contact damping. Based on previous work [8 - 10], the effective mass is assumed to be the mass of two chain links in the present study. The stiffness coefficient is calculated by linearizing the nonlinear function developed by Dubowsky and Freudenstein [25]. The damping is assumed to be viscous and the coefficient is taken as 0.1 for normally lubricated chain. The relative velocity is calculated approximately as follows [17].

$$V_{rel} = \omega_1 p_c \tag{2-2}$$

The effective mass can be considered as a small mass m_i moving with velocity V_{rel} and about to contact the surface of a sprocket tooth with an angle η between the surface and the direction of V_{rel} as shown in figure 1. The angle is determined by the contact point of the engaging roller. The contact point of the engaging roller remains very close to the transition point staying in the working curve close to the border between the seating curve and the working curve [26, 27]. Thus the angle is derived using the theoretical pressure angle.

$$\eta = 35 + \frac{240}{n_1} + \varepsilon \text{ (degrees)} \qquad (2\text{-}3)$$

where $\varepsilon << 1$.

A single impact between two elastic bodies is assumed to occur while the roller is in contact with the sprocket tooth surface. The component of the contact force in the chain span direction is the dynamic load due to the impact. The detailed derivation is in Appendix I. From Appendix I, the dynamic load for one tooth period is

$$D_{imp} = \frac{V_{rel} \sin 2\eta}{2\omega_d} e^{-\zeta\omega_n t} \{ (k_i - c_i \zeta \omega_n) \sin \omega_d t + c_i \omega_d \cos \omega_d t \} \quad (0 < t < \frac{\pi}{\omega_d}) \qquad (2\text{-}4\text{-}a)$$

$$D_{imp} = \quad 0 \qquad (\frac{\pi}{\omega_d} < t < \frac{\pi}{\omega_1 n_1}) \qquad (2\text{-}4\text{-}b)$$

The shape of D_{imp} is represented in figure 1.

Chains are often used in applications where the external loads are cyclic in nature, e.g. camshaft drives and intermittent motion machinery. The frequency of the load can vary from one cycle in a number of sprocket revolutions, to many cycles per revolution. In this paper the external load is modeled as previously suggested by Ulsoy, Whitesell, and Hooven [28]. The load comprises one cosine term.

$$D_{ext} = T_{ex} \cos \omega_{ex} t \qquad (2\text{-}5)$$

2.1.2 Polygonal Action

Two models were developed to compute dynamic load due to polygonal action. One is based on a rigid four bar mechanism and is used for the analysis of chain drives at low operating speeds. The other is based on an elastic four bar mechanism and is used for the analysis of chain drives at medium and high operating speeds.

a) Dynamic load based on rigid four bar model (applicable to low speeds)

In order to calculate the dynamic load, the angular velocity of the driven sprocket is needed. It is assumed that the angular velocity of the driving sprocket is constant. The fractional pitch is necessary for the representation of the phase between engagement and disengagement. The fractional pitch is defined as

$$f_p = \frac{L_{ct} - i*p_c}{p_c} \tag{2-6}$$

where i is any integer such that $0 \le f_p \le 1$.

The additional fractional pitch that is dependent on the operating speed [12] is not considered in this study. The angular velocity relationship between the driving and driven sprockets is given by the following equation (see figure 2) when chain velocity is assumed not to be affected by span vibration.

$$\omega_2 r_2 \sin\theta_2 = \omega_1 r_1 \sin\theta_1 \tag{2-7}$$

$$\text{Feasible domains}: \frac{\pi}{2} - \frac{\pi}{n_1} \le \theta_1 \le \frac{\pi}{2} + \frac{\pi}{n_1}, \quad \frac{\pi}{2} - \frac{\pi}{n_2} \le \theta_2 \le \frac{\pi}{2} + \frac{\pi}{n_2}$$

$$\text{where } \theta_1 = \omega_1 t + \frac{\pi}{2} - \frac{\pi}{n_1},\ \theta_2(0) = \frac{\pi}{2} - \frac{\pi}{n_2} + \alpha_f,\ \alpha_f = \frac{2\pi}{n_2} f_p .$$

In order to solve equation (2-7) for ω_2, the value of θ_2 must be obtained first. Equation (2-7) is integrated to get

$$\theta_2 = \theta_{2int} \qquad (\theta_{2int} \le \frac{\pi}{2} + \frac{\pi}{n_2}) \tag{2-8-a}$$

$$\theta_2 = \theta_{2int} - \frac{2\pi}{n_2} \qquad (\theta_{2int} > \frac{\pi}{2} + \frac{\pi}{n_2}) \tag{2-8-b}$$

$$\text{where } \theta_{2int} = \cos^{-1}\left\{\frac{r_1}{r_2}(\cos\theta_1 - \cos\theta_{10}) + \cos\theta_{20}\right\},$$

$$\theta_{10} = \theta_1(0) = \frac{\pi}{2} - \frac{\pi}{n_1},\ \theta_{20} = \theta_2(0) = \frac{\pi}{2} - \frac{\pi}{n_2} + \alpha_f.$$

With the obtained value of θ_2, ω_2 can be computed using equation (2-7). The angular acceleration of the driven sprocket (α_2) is obtained by differentiating equation (2-7) and the dynamic load is calculated considering the moment equilibrium about the driven sprocket shaft.

$$\alpha_2 = \frac{1}{r_2 \sin\theta_2}(r_1 \omega_1^2 \cos\theta_1 - r_2 \omega_2^2 \cos\theta_2) \tag{2-9}$$

$$D_{pol} = \frac{I_2}{r_2} \alpha_2 \tag{2-10}$$

The angular velocity of the driven sprocket and the dynamic load due to polygonal action are shown in figure 3 for three cases - (a) $n_1 = n_2$, (b) $n_1 > n_2$, and (c) $n_1 < n_2$. The magnitude of the dynamic load increases as the operating speed increases. The shape of the load is determined by the inverse ratio of the sprocket tooth numbers (n_2/n_1).

b) Dynamic load based on elastic four bar model

As the operating speed increases, the elasticity of chain span becomes important. The following analysis of the dynamic load takes the elasticity into consideration. It is assumed that the driving sprocket runs at a constant speed of ω_1. The reference axes, taken at O_1 are parallel and perpendicular to the common tangent to the pitch circles of the sprockets. The change of slope of the chain is neglected. Since the quantity $r_1 \sin\theta_1$ is a function of tooth period τ ($= 2\pi/(n_1\omega_1)$), it can be expressed as a Fourier series.

$$r_1 \sin\theta_1 = \frac{n_1 r_1}{\pi (1 - i^2 n_1^2)} \sin\frac{\pi}{n_1} + \sum_{i=1}^{\infty} \frac{2 n_1 r_1}{\pi (1 - i^2 n_1^2)} \sin\frac{\pi}{n_1} \cos ipt \tag{2-11}$$

where $p = n_1 \omega_1$.

It is approximated up to second harmonic terms considering that the values of the coefficients decrease rapidly as the order of the harmonic increases.

$$r_1 \sin\theta_1 \approx a_0 + a_1 \cos pt + a_2 \cos 2pt \tag{2-12}$$

$$\text{where } a_0 = \frac{n_1 r_1}{\pi} \sin\frac{\pi}{n_1}, \quad a_1 = \frac{2 a_0}{1 - n_1^2}, \quad a_2 = \frac{2 a_0}{1 - 4 n_1^2}.$$

The speed of A_1 is given by

$$\dot{x}_1 \approx - \omega_1 (a_0 + a_1 \cos pt + a_2 \cos 2pt)$$

and by integration

$$x_1(t) \approx -\omega_1 \left(a_0 t + \frac{a_1}{p} \sin pt + \frac{a_2}{2p} \sin 2pt\right) + x_1(0) \qquad (2\text{-}13)$$

In a similar manner it can be shown that

$$r_2 \sin\theta_2 \approx N a_0 + b_1 \cos pt + c_1 \sin pt + b_2 \cos 2pt + c_2 \sin 2pt \qquad (2\text{-}14)$$

where $b_1 = \frac{2 N a_0}{1 - n_2^2} \cos n_2\alpha$, $c_1 = -\frac{2 N a_0}{1 - n_2^2} \sin n_2\alpha$, $b_2 = \frac{2 N a_0}{1 - 4 n_2^2} \cos 2n_2\alpha$,

$$c_2 = -\frac{2 N a_0}{1 - 4 n_2^2} \sin 2n_2\alpha, \quad N = \frac{n_2}{n_1} = \frac{\frac{n_2 r_2}{\pi} \sin(\frac{\pi}{n_2})}{\frac{n_1 r_1}{\pi} \sin(\frac{\pi}{n_1})}.$$

Equation (2-14) was derived based on the assumption that the speed of the driven sprocket is constant. In fact the speed is subject to small fluctuations but it can be shown that the error involved in equation (2-14) is negligible.

Let the speed of A_2 be given by

$$\dot{x}_2 = -\frac{\omega_1}{N} (N a_0 + l_1 \cos pt + m_1 \sin pt + l_2 \cos 2pt + m_2 \sin 2pt) \qquad (2\text{-}15)$$

Integrating equation (2-15) and substituting boundary conditions, we get

$$x_2(t) = -\frac{\omega_1}{N} \left(N a_0 t + \frac{l_1}{p} \sin pt - \frac{m_1}{p} \cos pt + \frac{l_2}{2p} \sin 2pt - \frac{m_2}{2p} \cos 2pt\right) \qquad (2\text{-}16)$$

$$-\frac{\omega_1}{N p} \left(m_1 + \frac{m_2}{2}\right) + x_1(0) + L$$

Now the angular velocity of the driven sprocket is calculated noting that b_1, b_2, c_1 and c_2 are small quantities and the angular acceleration is obtained by differentiating the angular velocity.

$$\dot{\theta}_2 = -\frac{\dot{x}_2}{r_2 \sin\theta_2} \approx \frac{\omega_1}{N^3 a_0^2} (N a_0 + l_1 \cos pt + m_1 \sin pt + l_2 \cos 2pt + m_2 \sin 2pt)$$
$$(N a_0 - b_1 \cos pt - c_1 \sin pt - b_2 \cos 2pt - c_2 \sin 2pt) \qquad (2\text{-}17)$$

$$\ddot{\theta} = \frac{d}{dt}(\dot{\theta}) \tag{2-18}$$

For oscillations of the driven system about the axis of rotation, the equation of motion is

$$I_2 \ddot{\theta}_2 + k (x_1 + L - x_2) r_2 \sin \theta_2 = 0 \tag{2-19}$$

where I_2 : moment of inertia of driven system about axis of rotation,

$k = \frac{AE}{L}$, AE = strength of chain span.

Substituting equations (2-13), (2-14), (2-16), and (2-18) into equation (2-19) and letting each term related with each harmonic be zero, a set of algebraic equations are obtained.

$$\mathbf{A\ X = F} \tag{2-20}$$

where **X** is a 4×1 matrix whose elements are unknown variables (l_1, m_1, l_2,m_2).

The elements for the matrices are shown in Appendix II.

There are four unknowns and nine equations, resulting in an over-determined system. Since there is no exact solution, an approximate solution is achieved using a least squares method.

$$\mathbf{X} = (\mathbf{A}^T \mathbf{A})^{-1} \mathbf{A}^T \mathbf{F} \tag{2-21}$$

Based on the values of l_1, m_1, l_2, m_2 obtained above, the dynamic load is calculated as follows.

$$D_{pol} = k (x_2 - x_1 - L) = \frac{k \omega_1}{N p} \{(N a_1 - l_1) \sin pt + m_1 \cos pt + 0.5 (N a_2 - l_2) \sin 2pt + 0.5 m_2 \cos 2pt - m_1 - 0.5 m_2\} \tag{2-22}$$

θ_2 is obtained by integrating equation (2-17) symbolically.

$$\theta_2 = \int_0^t \dot{\theta}_2\, dt = \frac{\omega_1}{N^3 a_0^2}(q_0 t + q_1 \sin pt + q_2 \sin 2pt + q_3 \sin 3pt + q_4 \sin 4pt$$
$$- p_0 t - p_1 \cos pt - p_2 \cos 2pt - p_3 \cos 3pt - p_4 \cos 4pt + c_{int}) \quad (2\text{-}23)$$

$$\text{where } c_{int} = \frac{N^3 a_0^2}{\omega_1}(\alpha_f + \frac{\pi}{2} - \frac{\pi}{n_2}) + p_1 + p_2 + p_3 + p_4 - q_0 \tau\, \text{dint}(\frac{t}{\tau}),$$

dint(x) rounds the value of x to the nearest integer towards zero.

The coefficients including q_i, and p_i are shown in Appendix III.

In addition, there is an abrupt length change in chain span except when the length of the common tangent is equal to an integral number of pitches. The length increases by one pitch when the chain link disengages from the driven sprocket and the length decreases by one pitch when the chain link engages with the driving sprocket. This length change causes a change in the longitudinal stiffness of the span thus introducing a sudden change in the dynamic load due to polygonal action.

$$L = L_0 \rightarrow k = k_1 = \frac{AE}{L_1}, \quad L = L_0 + p_c \rightarrow k = k_2 = \frac{AE}{L_2}$$

Therefore there are two system characteristic resonances in the dynamic load corresponding to the two cases ($k = k_1$ and $k = k_2$) in contrast with [6] where there was only one. Furthermore, the magnitude of the dynamic load is limited around the resonances while the magnitude was unlimited in [6]. The magnitude change of the dynamic load along with the change of the operating speed and various shapes of the dynamic loads are shown in figure 4. The two resonances (ω_{c1} and ω_{c2}) can cause Mathieu type dynamic instabilities of chain drive system. The existence and the positions of the peaks, if they exist, are determined by operating speed and system characteristics including longitudinal stiffness of chain span, the inverse ratio of the sprocket tooth numbers, and moment of inertia of the driven sprocket system.

2.2 Transverse Displacements of End Points and Periodic Length Change

There are two end points for a chain span, one associated with each sprocket. Each end point is moving along an arc formed by one tooth angle ($2\pi/n_1$ or $2\pi/n_2$) and there is generally a phase shift between the two periodic motions of the end points. The vertical motions (u_n, u_0) of the end points are approximated as

$$u_n = r_1 (1 - \sin \theta_1) \tag{2-24}$$

where $\theta_1 = \omega_1 t + \frac{\pi}{2} - \frac{\pi}{n_1}$.

$$u_0 = r_2 (1 - \sin \theta_2) \tag{2-25}$$

The value of θ_2 is determined by either equation (2-8) or (2-23). Both u_n and u_0 are shifted by - 0.5 r_2 (1 - cos (π/n_2)) in order to consider the proper shapes of the displacement excitations in the computer simulation. As mentioned in section 2.1.2.(b), there is a length change in general chain drive operation. The length change occurs either at the engagement of the chain link or the disengagement. When θ_1 goes beyond its limit $\pi/2 + \pi/n_1$ (engagement), the free span length decreases by one pitch. When θ_2 goes beyond its limit $\pi/2 + \pi/n_2$ (disengagement), the span length increases by one pitch. This length change affects not only the shape of the dynamic load due to polygonal action but also the transverse vibration of chain drive.

2.3 Equations of Motion

It is proposed here that a chain drive system can be modeled as a moving uniform string and that the discrete nature (polygonal action and impact phenomenon) can be incorporated into the system equation of motion through the tension term and the boundary conditions.

2.3.1 General Equations of Motion

The general equations of motion for an axially moving chain span are derived in two-dimensional space using Hamilton's principle following the similar procedure in reference [29]. Strain energy, gravitational potential energy and kinetic energy are formulated. There is external work due to both the static tension and the dynamic tensions (speed tensioning, polygonal action, impact and external periodic load) and the work is done to the chain span through both ends.

Two equations of motion are derived for both longitudinal and transverse motions.

$$\begin{aligned} u_1 : \; & \{(P^e + E A^e \varepsilon) a_1\}_{,S} - (P^e + E A^e \varepsilon) \kappa^e a_2 - \rho A^e g l_1 \\ & = \{\rho A^e (u_{1,t} + c^e a_1)\}_{,t} + \{\rho A^e c^e (u_{1,t} + c^e a_1)\}_{,S} - \rho A^e c^e \kappa^e (u_{2,t} + c^e a_2) \end{aligned} \tag{2-26}$$

$$\begin{aligned} u_2 : \; & \{(P^e + E A^e \varepsilon) a_2\}_{,S} + (P^e + E A^e \varepsilon) \kappa^e a_1 - \rho A^e g l_2 \\ & = \{\rho A^e (u_{2,t} + c^e a_2)\}_{,t} + \{\rho A^e c^e (u_{2,t} + c^e a_2)\}_{,S} + \rho A^e c^e \kappa^e (u_{1,t} + c^e a_1) \end{aligned} \tag{2-27}$$

where S : arc length coordinate measured along the chain span,

u_1, u2 : the displacement along and perpendicular to the chain span from the equilibrium respectively

$$\varepsilon = u_{1,S} - \kappa^e u_2 + \frac{1}{2}\{(u_{1,S} - \kappa^e u_2)^2 + (u_{2,S} + \kappa^e u_1)^2\},$$

$$a_1 = 1 + u_{1,S} - \kappa^e u_2, \quad a_2 = \kappa^e u_1 + u_{2,S},$$

$$P^e = \sqrt{\{(P_0 - m_1 c^{e2})^2 + (m_1 g \overline{S^e})^2\}} + m_1 c^{e2}, \quad \kappa^e = \frac{m_1 g (P_0 - m_1 c^{e2})}{(P_0 - m_1 c^{e2})^2 + (m_1 g \overline{S^e})^2},$$

P^e : tension of chain span at equilibrium configuration,

P_0 : tension of the lowest point of chain span at equilibrium configuration,

κ^e : curvature at equilibrium configuration.

$\overline{S^e}$: span length from the lowest point at equilibrium

There are two geometric boundary conditions ($u_2(0,t)$, $u_2(L^e,t)$) calculated through the kinematic analysis of chain span and two natural boundary conditions related with longitudinal motion.

$u_2(0,t)$, $u_2(L^e,t)$: prescribed

$-(P^e + E A^e \varepsilon) a_1 + P_1 = 0$ at $S^e = 0$

$-(P^e + E A^e \varepsilon) a_1 + P_2 = 0$ at $S^e = L^e$

2.3.2 Equation of Motion for Chain Drive at Low and Medium Speeds

In most applications of chain drives at low operating speeds, there exists a small sag[1] in the chain span. The nonlinear equations of motion about the equilibrium configuration are obtained from (2-26) and(2-27). The superscript e is dropped out from here forward.

$$u_1 : \{(E A \varepsilon + (P + E A \varepsilon)(u_{1,S} - \kappa u_2)\}_{,S} - (P + E A \varepsilon) \kappa (u_{2,S} + \kappa u_1)$$
$$= [m_1 \{u_{1,t} + c (u_{1,S} - \kappa u_2)\}]_{,T} + [m_1 c \{u_{1,T} + c (u_{1,S} - \kappa u_2)\}]_{,S}$$
$$- m_1 c \kappa \{u_{2,t} + c (u_{2,S} + \kappa u_1)\} \qquad (2\text{-}28)$$

---

[1] The boundary between small and large sags is determined in terms of sag-span ratio (sag/ span length). As a rule of thumb, small sag theory holds when the sag-span ratio is less than 1/8.

$$u_2 : \{(P + E\,A\,\varepsilon)\,(u_{2,S} + \kappa\,u_1)\}_{,S} + \kappa\,\{E\,A\,\varepsilon + (P + E\,A\,\varepsilon)\,(u_{1,S} - \kappa\,u_2)\}$$
$$= [m_l\,\{u_{2,t} + c\,(u_{2,S} + \kappa\,u_1)\}]_{,t} + [m_l\,c\,\{u_{2,t} + c\,(u_{2,S} + \kappa\,u_1)\}]_{,S}$$
$$+ m_l\,c\,\kappa^e\,\{u_{1,t} + c\,(u_{1,S} - \kappa\,u_2)\} \qquad (2\text{-}29)$$

With the small sag assumption, the curvature and the tension at equilibrium are approximated up to order of δ ($\sim m_l\,g\,L_c/(P_0 - m_l\,c^2)$).

$$P = \sqrt{\{(P_0 - m_l\,c^2)^2 + (m_l\,g\,\bar{S})^2\}} + m_l\,c^2 \approx P_0 \qquad (2\text{-}30)$$

$$\kappa = \frac{m_l\,g\,(P_0 - m_l\,c^2)}{(P_0 - m_l\,c^2)^2 + (m_l\,g\,\bar{S})^2} \approx \frac{m_l\,g}{P_0 - m_l\,c^2} = \frac{\delta}{L_c} \qquad (2\text{-}31)$$

where L_c = total curved span length.

Assume that the chain stretches in a quasi-static manner ($E\,A >> P$) and linearize the equation of motion for u_1 component to get

$$(E\,A\,\varepsilon)_{,S} = 0 \qquad (2\text{-}32)$$

Thus the dynamic component of chain tension becomes

$$f(t) = E\,A\,\varepsilon = E\,A\,(u_{1,S} - \kappa\,u_2) \qquad (2\text{-}33)$$

At both ends,

$$f(t) = P_t = E\,A\,(u_{1,S} - \kappa\,u_2) \qquad (2\text{-}34)$$

The tangential displacement is obtained by integrating equation (2-34) and removing the rigid body mode.

$$u_1 = \kappa\left(\int_0^S u(\eta,t)\,d\eta - \int_0^{L_c} u(\eta,t)\,d\eta\right) + \frac{P_t}{EA}(S - L_c) \qquad (2\text{-}35)$$

Linearizing the equations of motion for u_2 component about the quasi-static solution and including viscous damping in transverse direction gives

$$m_1 u_{2,tt} + 2 m_1 c u_{2,tS} + m_1 c^2 u_{2,SS} + c_d(u_{2,t} + c u_{2,S}) - \{(P + P_t) u_{2,S}\}_{,S} - \kappa P_t = 0 \qquad (2\text{-}36)$$

where $P = T_s + \lambda m c^2$, $P_t = D_{pol} + D_{imp} + D_{ext}$.

There are both parametric and external excitations in the system equation of motion. In the case of negligible sag, the equation of motion becomes

$$m_1 u_{2,tt} + 2 m_1 c u_{2,tx} + m_1 c^2 u_{2,xx} + c_d(u_{2,t} + c u_{2,x}) - \{(P + P_t) u_{2,x}\}_{,x} = 0 \qquad (2\text{-}37)$$

Equations (2-36) and (2-37) are not simple parabolic or hyperbolic partial differential equations but mixed type partial differential equations with time dependent coefficients and time dependent boundary conditions. In order to solve the equations of motion, a finite difference method was adopted. Central finite differencing was done about time and mixed finite differencing was done about the spatial coordinate. The mixed finite differencing combines central differencing at low operating speeds and backward differencing at high speeds [28]. Accordingly, the first derivative for the spatial coordinate is expressed as

$$\frac{\partial u}{\partial S} = \frac{1 - s^*}{2\,\Delta S} u_{i+1,j} + \frac{s^*}{\Delta S} u_{i,j} - \frac{1 + s^*}{2\,\Delta S} u_{i-1,j} \qquad (2\text{-}38)$$

where i = subscript for spatial coordinate,

j = subscript for time, $s^* = \dfrac{c}{\sqrt{T_s/m_1}}$.

2.3.3 Equations of Motion for Chain Drive at High Operating Speeds

As the operating speed approaches the first resonance of longitudinal motion, the quasi-static assumption no longer holds and equations (2-28) and (2-29) should be solved simultaneously. When a chain drive is operated at such high speeds, sag is usually not allowed in practice. There are two cases where the simultaneous solution of the two equations is required. The first case occurs when the tooth frequency dependent loads have a significant effect on the coupling between the transverse and longitudinal equations of motion and the tooth frequency is near the first longitudinal resonant frequency. The second case occurs when the frequency of the external load is an integral multiple of the

frequency of rotation of the driving sprocket, this frequency is near the first longitudinal resonance, and the amplitude of the external excitation is large enough to make the coupling term significant. This case does not happen unless the operating speed of the chain drive is very high.

The nonlinear equations of motion of a chain with an arbitrary sag are expressed about the equilibrium configuration by equations (2-28) and (2-29). Several modifications are required to obtain the equations of motion for the chain without sag, specifically

$$\kappa = 0,\ S = x,\ a_1 = 1 + u_{1,x},\ a_2 = u_{2,x},\ \varepsilon \approx u_{1,x} + \frac{1}{2} u_{2,x}^2 \quad (E A >> P)$$

With those modifications and the addition of viscous damping in the transverse direction, the equations of motion and boundary conditions can be obtained. The mode shapes for an axially stationary string are taken as the comparison functions for the transverse vibration. Suitable comparison functions for the longitudinal vibration are not readily determined, so admissible functions defined by the longitudinal vibration modes of a free-free rod are used.

$$u_1 = \sum_{j=1}^{N} \psi_j(t) \cos \frac{j \pi x}{L}, \quad u_2 = \sum_{j=1}^{N} \phi_j(t) \sin \frac{j \pi x}{L} + \frac{L - x}{L} g(t) + \frac{x}{L} h(t) \qquad (2\text{-}39)$$

where $g(t) = u_2(0,t)$, $h(t) = u_2(L,t)$.

Since the admissible functions are used in the discretization process, the discretization from the variational form was done. The variational form for the chain drive without sag is obtained from the original Hamilton's formulation with several modifications including viscous damping in the transverse direction.

$$\begin{aligned} u_1 : \int_{t_1}^{t_2} \Big[\int_0^L \{ -m_1 (u_{1,tt} + 2 c u_{1,xt} + c^2 u_{1,xx}) + E A u_{1,xx} + E A u_{2,x} u_{2,xx} \} \delta u_1 \, dx \\ + \{ E A (u_{1,x} + \frac{1}{2} u_{2,x}^2) - P_t \} \delta u_1 |_{x=0} + \{ -E A (u_{1,x} + \frac{1}{2} u_{2,x}^2) \\ + P_t \} \delta u_1 |_{x=L} \Big] dt = 0 \end{aligned} \qquad (2\text{-}40)$$

$$u_2 : \int_{t_1}^{t_2} \int_0^L [-m_l (u_{2,tt} + 2\, c\, u_{2,xt} + c^2\, u_{2,xx}) + P\, u_{2,xx} - c_d (u_{2,t} + c\, u_{2,x}) + E\, A \{u_{1,xx}\, u_{2,x} + u_{1,x}\, u_{2,xx} + 1.5\, u_{2,x}^2\, u_{2,xx}\}] \delta u_2\, dx = 0 \quad (2\text{-}41)$$

The final form of the discretized equations of motion was obtained by substituting expressions (2-39) into equations (2-40) and (2-41). The discretized equations of motion are a set of nonlinearly coupled second order ordinary differential equations and the Runge-Kutta fourth order method was used as an integration scheme.

3. COMPUTER SIMULATION

3.1 Time Step Control and Simulation Strategy

A nonuniform time step scheme was developed to execute computation efficiently. The basic objective of the scheme is to use smaller time steps near the instant of the impact (between engaging roller and sprocket tooth) and larger time steps away from that instant so that the effect of the impact is included while the total computation time is minimized without causing numerical instabilities. To achieve this objective, an exponential function was utilized.

The main objective of the simulation is to observe the change of the vibration amplitude of the roller chain drive under different circumstances. In order to obtain the steady state response at each operating speed, the transient region during some amount of time from the beginning was ignored and the response after that was used to calculate the vibration amplitude. The chain motion is complex. For purpose of the discussion, it is desirable to characterize this complex motion by a single descriptor. Our experience indicates that a good choice for this descriptor is the maximum amplitude from the chain span equilibrium position. This variable can illustrate the vibration effectively over a wide range of operating speeds.

3.2 Simulation Results and Discussion

A specific chain drive system was selected for detailed study. It included one number 40 chain and two 24 tooth sprockets. The center distance ranged from 19.7 pitches to 20.5 pitches. First simulation was done to investigate the effect of periodic length change and the center distance on the vibration response. Figure 5 shows both effects. The solid line represents the simulation results obtained considering a center distance as an average span length and the dashed line represents the results obtained including periodic length change

in chain span. The difference becomes clearer as the operating speed approaches high order resonances. When there is no consideration of the length change, one peak of the vibration amplitude occurs at each order resonance for the center distance. In contrast, when the periodic length change is considered, two peaks occur at each order resonance (one for the short length and one for the long length) except in the case where the center distance is an integral number of the pitches. Other peaks also exist near the two peaks. The reason for the other peaks is the effect of the dynamic load due to the polygonal action combined with the periodic length change. The effect of center distance becomes clear when the system with 20 pitch center distance (system A) is compared with the system with 20.5 center distance (system B). The response of the system A was clearly amplified but the one of the system B was not amplified around the first resonance. This result is in agreement with the results of previous discrete approaches ([10], [12]). The reason is that the transverse displacements at both ends of system A are in phase, thus exciting the first mode properly. However, the displacements of system B are out of phase and can not efficiently excite the first mode. As shown in the observation of vibration amplitudes at the first resonance, center distance has a major influence on the positions of higher resonances and the vibration amplitudes. Since the amplitude at a specific operating speed is affected significantly by the center distance, the optimal center distance should be decided by the speed at which the system is operated.

In addition to the transverse displacement excitations at both ends of the chain span, there are other intrinsic excitations which correspond to dynamic loads due to polygonal action and impact. The effect of polygonal action is dominant at low and medium speeds while the effect of impact is dominant at high operating speed. The magnitude of the tension variation due to the polygonal action depends on the moment of inertia of the driven sprocket system and operating speed. The first effect of the parametric excitation due to the tension variation is the increase of the amplitudes around the resonances as shown in figure 6a. The second effect is well represented in figure 6b and the other peaks besides the two peaks for the short and the long length start to appear as the moment of inertia increases. Figure 7 shows the effect of static tension. As the magnitude of the static tension decreases, the possibility of the instabilities due to the dynamic load by the polygonal action increases. In the first two cases (figure 7a and b), no instabilities were observed while in the third and fourth cases, the instabilities occur. Thus low static tension can give lower loads to the shaft bearing up to some point, but excessively low static tension can cause instabilities due to the combined effect of both parametric and external excitations.

The external periodic loads were observed to change the excitation frequency and the magnitude. The common effect for all cases considered here is that the addition of external

periodic loads reduces the vibration amplitude around resonances and increases the amplitude away from resonances. The effect of different excitation frequencies is shown in figure 8. The frequency changes from $4\omega_1$ to ω_1 and the effect of external load increases as the frequency decreases. Also, the effects of external load increase as the amplitude of the external load increases.

The motion of a chain drive at medium operating speeds is characterized by the dynamic load due to polygonal action based on the elastic four bar mechanism. There are two possible instabilities due to the dynamic load. The existence of the instabilities is limited by the operating speed, the inverse ratio of the sprocket tooth numbers, and the moment of inertia for the driven sprocket system. Figure 9 shows both the cases with and without the instabilities. The possibility of the instabilities increases as the ratio becomes larger and the moment of inertia becomes smaller.

The behavior of the chain drive near the first longitudinal resonance is observed in figure 10 which was produced by solving both equations of motion for transverse and longitudinal vibrations simultaneously. The vibration amplitudes near the first longitudinal resonance and near the fifth transverse resonance (located a little above the longitudinal resonance) were observed. The vibration amplitude is only weakly amplified near the first resonance because the magnitude of the dynamic load due to polygonal action is very small and the fundamental component of the dynamic load due to impact is not very large. However, the coupling between the longitudinal vibration and the transverse vibration is very clear near the transverse resonance. Accordingly it is suggested that operation near the transverse resonance close to the first longitudinal resonance should be avoided.

4. SUMMARY AND CONCLUSION

The chain drive model presented here includes several important features such as impact phenomenon, polygonal action, periodic length change, external periodic loads and nonlinear coupling between transverse and longitudinal motions at high operating speeds. At low operating speeds, the polygonal action and the external periodic loads govern the vibration characteristics largely through the transverse displacement excitations and the periodic tension variations. For a given center distance, there are two major peaks in the vicinity of each linear resonance (one before and one after). These peaks correspond to the short and long chain span lengths. There are also other peaks due to the combined effects of both parametric and external excitation. The vibration responses are affected by center distances over a wide range and the instabilities around the linear resonances can occur due to the periodic tension variation. The external periodic load with a frequency of the rotating speed of the driving sprocket can reduce the amplitudes around the resonances and increase

the amplitude away from the resonances. At medium operating speeds, there is a danger of instabilities due to the two resonances of the dynamic load due to polygonal action. But the instabilities do not always occur. The possibility of instabilities increases as the ratio of n_2/n_1 becomes larger and the moment of inertia for the driven sprocket system becomes smaller. At high operating speeds, the coupling between transverse and longitudinal vibrations is not significant around the first longitudinal vibration because of the small magnitude of the excitation but the coupling between them is clear around the transverse resonance slightly above the longitudinal resonance.

The suggested model still has its limitations and in order to investigate the vibration characteristics of roller chain drives more exactly, refined models of impact and polygonal action interacting with span vibration should be developed. Experimental work will be necessary to augment the theoretical work.

5. ACKNOWLEDGEMENTS

The authors gratefully acknowledge the support of the National Science Foundation through Grants No. MSM-88-12957 and MSS-8996293. We also wish to thank N. C. Perkins for his thoughtful suggestions during the early stage of the model development.

BIBLIOGRAPHY

1. Jackson and Moreland, "Design Manual for Roller and Silent Chain Drives", Association of Roller and Silent Chain Manufactures, 1955, 95 pp.
2. K. W. Wang, "On the Stability of Chain Drive Systems Under Periodic Sprocket Oscillations", ASME J. of Vibration and Acoustics, vol. 114, Jan., 1992, pp.119 - 126.
3. R. A. Morrison, "Polygonal Action in Chain Drives," Machine Design, vol. 24, no. 9, 1952, pp.155 - 159.
4. G. Bouillon and G. V. Tordian, "On Polygonal Action in Roller Chain Drives," ASME Transactions, vol. 87, 1965, pp.243 - 250.
5. C. K. Chen and F. Freudenstein, "Toward a More Exact Kinematics of Roller Chain Drives", ASME Journal of Mechanism, Transmission, and Automation in Design, Sept. 1988, vol. 110, pp.269-275.
6. S. Mahalingam, "Polygonal Action in Chain Drives", J. Franklin Inst., vol. 265, no. 1, 1958, pp.23 - 28.
7. S. R. Turnbull and J. N. Fawcett, "An Approximate Kinematic Analysis of the Roller Chain Drive", Proc. Fourth World Congress on the Theory of Machines and Mechanisms, 1975, paper no. 168.
8. G. K. Ryabov, "Inertia Effects of Impact Loading in Chain Drive", Russian Engineering

Journal, vol. 48, No. 8, pp.17-19.
9. M. Chew, "Inertia Effects of a Roller Chain on Impact Intensity", ASME J. of Mechanism, Transmission, and Automation in Design, vol. 107, Mar. 1985, pp.123 - 130.
10. S. R. Turnbull and J. N. Fawcett, "Dynamic Behavior of Roller Chain Drives," Instn. Mech. Engrs., 1973, pp.29 - 35.
11. J. W. Fawcett and S. W. Nicol, " A Theoretical Investigation of the Vibration of Roller Chain Drives", Proc. Fifth World Congress on the Theory of Machines and Mechanisms, 1979, pp. 1482 - 1485.
12. M. Kim, "Dynamic Behavior of Roller Chain Drives at Moderate and High Speeds", Ph. D. dissertation, The University of Michigan, 1990, 122 p.
13. K. W. Wang, S. P. Liu, S. I. Hayek, and F. H. K. Chen, "On the impact intensity of Vibrating Axially Moving Roller Chains", vol. 114, Jul., 1992, pp.397 - 403.
14. J. C. Conwell, G. E. Johnson, and S. W. Peterson, "Design and Construction of a Machine to Evaluate the Forces in Roller Chain Drives", Proceedings of the 1992 International Power Transmission and Gearing Conference, DE-vol. 43-2, ASME 1992, pp.703-709.
15. J. C. Conwell, G. E. Johnson, and S. W. Peterson, "Experimental Investigation of the Forces in a Link Side Plate During Normal Operation of a Roller Chain Drive", Proceedings of the 1992 International Power Transmission and Gearing Conference, DE-vol. 43-2, ASME 1992, pp.711-716.
16. J. C. Conwell, G. E. Johnson, and S. W. Peterson, "Experimental Investigation of the Impact Force that Occurs When a Roller Seats on the Sprocket During Normal Operation of a Roller Chain Drive", Proceedings of the 1992 International Power Transmission and Gearing Conference, DE-vol. 43-2, ASME 1992, pp.717-721.
17. R. C. Binder, "Mechanics of the Roller Chain Drive", Prentice-Hall, 1956, 204 p.
18. Y. Tsujioka, " Transverse Vibration of Roller Chain", Trans. JSME, vol. 42, no. 356, 1976, pp.1087 - 1095.
19. N. C. Veikos and F. Freudenstein, "On the Dynamic Analysis of Roller Chain Drives : Part 1- Theory", Mechanism Design and Synthesis, DE-vol. 46, edited by Kinzel et al, ASME, NY, 1992, pp.431-438.
20. H. Shimizu and A. Sueoka, "Nonlinear Forced Vibration of Roller Chain," Bull. JSME, vol. 18, no. 124, 1975, pp. 1090 - 1100.
21. S. Mahalingam, "Transverse Vibrations of Power Transmission Chains," Brit. J. Appl. Phys., vol. 8, 1957, pp.145 - 148.
22. S. Naguleswaran and C. J. H. Williams, "Lateral Vibrations of Bandsaw Blades,

Pulley Belts, and the like," Int. J. Mech. Sciences, vol. 10, 1968, pp.239 - 250.
23. S. T. Ariaratnam and S. F. Asokanthan, "Dynamic Stability of Chain Drives", Trans. ASME Journal of Mechanism, Transmission, and Automation in Design, vol.109, no. 3, 1987, pp.412 - 418.
24. C. D. Mote, Jr., "Some Dynamic Characteristics of Band Saws", Forest Products Journal, January 1965, pp.37-41.
25. S. Dubowsky and F. Freudenstein, "Dynamic Analysis of Mechanical Systems with Clearances : Part 1 (Formulation of Dynamic Model)", ASME Journal of Engineering for Industry, Feb. 1971, pp.305 - 309.
26. M. Kim and G. E. Johnson, "Mechanics of Roller Chain-Sprocket Contact : A General Modelling Strategy", Proceedings of the 1992 International Power Transmission and Gearing Conference, DE-vol. 43-2, ASME 1992, pp.689 - 695.
27. M. Kim and G. E. Johnson, "Mechanics of Roller Chain-Sprocket Contact : Observations about the Contact Phenomena and Load Distribution", Proceedings of the 1992 International Power Transmission and Gearing Conference, DE-vol. 43-2, ASME 1992, pp.696 - 702.
28. A. G. Ulsoy, J. E. Whitesell, and M. D. Hooven, "Design of Belt-Tensioner Systems for Dynamic Stability", ASME Journal of Vibration, Stress, and Reliability in Design, vol.107, Jul. 1985, pp.282-290.
29. N. C. Perkins and C. D. Mote, "Three-dimensional Vibration of Travelling Elastic Cables", J. Sound and Vibration, vol. 114, no. 2, pp.325 - 340.

Appendix I

Derivation of Dynamic Load due to Impact

The component of contact force in the chain span direction is the dynamic load due to the impact and it is calculated assuming that the sprocket is stationary during the impact since the inertia of the sprocket is large comparing with m_i. When the roller is in contact with the tooth, its equation of motion is as follows [11].

$$m_i \ddot{x}_0 + c_i \dot{x}_0 + k_i x_0 = 0$$

Initial conditions : $x_0(0) = 0, \quad \dot{x}_0(0) = V_{rel} \sin \eta$

Then the solution is given by

$$x_0 = \frac{e^{-\zeta \omega_n t}}{\omega_d} V_{rel} \sin \eta \sin \omega_d t$$

where $\zeta = \frac{c_i}{2\sqrt{m_i k_i}}$, $\omega_n = \sqrt{\frac{k_i}{m_i}}$, $\omega_d = \omega_n\sqrt{1-\zeta^2}$.

And the solution applies until $x_0 = 0$ again.

$$\sin \omega_d t_i = 0 \ , \ t_i = \frac{\pi}{\omega_d}$$

Let the dynamic load due to the impact be D_{imp}.

$$D_{imp} = (c_i\dot{x}_0 + k_i x_0)\cos\eta = \frac{V_{rel}\sin 2\eta}{2\omega_d} e^{-\zeta\omega_n t}\{(k_i - c_i\zeta\omega_n)\sin\omega_d t + c_i\omega_d\cos\omega_d t\}$$

where $0 < t < t_i$.

Appendix II

Elements of Matrices in Equation (2-20) :

$$a_{11} = \frac{c_1 k \omega_1}{2 N p}, \quad a_{12} = \frac{a_0 k \omega_1}{p} - \frac{b_1 k \omega_1}{2 N p}, \quad a_{13} = \frac{c_2 k \omega_1}{4 N p}, \quad a_{14} = \frac{a_0 k \omega_1}{2 p} - \frac{b_2 k \omega_1}{4 N p},$$

$$a_{21} = \frac{c_2 k \omega_1}{2 N p} - \frac{c_2 I_2 p \omega_1}{2 a_0^2 N^3}, \quad a_{22} = -\frac{a_0 k \omega_1}{p} + \frac{b_1 k \omega_1}{N p} - \frac{b_2 k \omega_1}{2 N p} + \frac{b_2 I_2 p \omega_1}{2 a_0^2 N^3} + \frac{I_2 p \omega_1}{a_0 N^2},$$

$$a_{23} = \frac{c_1 k \omega_1}{4 N p} + \frac{c_1 I_2 p \omega_1}{2 a_0^2 N^3}, \quad a_{24} = \frac{b_1 k \omega_1}{4 N p} - \frac{b_1 I_2 p \omega_1}{2 a_0^2 N^3}, \quad a_{31} = -\frac{c_1 k \omega_1}{2 N p} - \frac{c_1 I_2 p \omega_1}{a_0^2 N^3},$$

$$a_{31} = -\frac{c_1 k \omega_1}{2 N p} - \frac{c_1 I_2 p \omega_1}{a_0^2 N^3}, \quad a_{32} = -\frac{b_1 k \omega_1}{2 N p} + \frac{b_2 k \omega_1}{N p} - \frac{b_1 I_2 p \omega_1}{a_0^2 N^3},$$

$$a_{32} = -\frac{b_1 k \omega_1}{2 N p} + \frac{b_2 k \omega_1}{N p} - \frac{b_1 I_2 p \omega_1}{a_0^2 N^3}, \quad a_{33} = 0, \quad a_{34} = -\frac{a_0 k \omega_1}{2 p} + \frac{b_2 k \omega_1}{2 N p} + \frac{2 I_2 p \omega_1}{a_0 N^2},$$

$$a_{41} = -\frac{c_2 k \omega_1}{2 N p} - \frac{3 c_2 I_2 p \omega_1}{2 a_0^2 N^3}, \quad a_{42} = -\frac{b_2 k \omega_1}{2 N p} - \frac{3 b_2 I_2 p \omega_1}{a_0^2 N^3}, \quad a_{43} = -\frac{c_1 k \omega_1}{4 N p} - \frac{3 c_1 I_2 p \omega_1}{2 a_0^2 N^3},$$

$$a_{43} = -\frac{c_1 k \omega_1}{4 N p} - \frac{3 c_1 I_2 p \omega_1}{2 a_0^2 N^3}, \quad a_{44} = -\frac{b_1 k \omega_1}{4 N p} - \frac{3 b_1 I_2 p \omega_1}{2 a_0^2 N^3}, \quad a_{51} = a_{52} = 0,$$

$$a_{53} = -\frac{c_2 k \omega_1}{4 N p} - \frac{2 c_2 I_2 p \omega_1}{a_0^2 N^3}, \quad a_{54} = -\frac{b_2 k \omega_1}{4 N p} - \frac{2 b_2 I_2 p \omega_1}{a_0^2 N^3},$$

$$a_{61} = \frac{a_0 k \omega_1}{p} - \frac{b_2 k \omega_1}{2 N p} + \frac{b_2 I_2 p \omega_1}{2 a_0^2 N^3} - \frac{I_2 p \omega_1}{a_0 N^2}, \quad a_{62} = \frac{c_1 k \omega_1}{N p} - \frac{c_2 k \omega_1}{2 N p} + \frac{c_2 I_2 p \omega_1}{2 a_0^2 N^3},$$

$$a_{63} = \frac{b_1 k \omega_1}{4 N p} + \frac{b_1 I_2 p \omega_1}{2 a_0^2 N^3}, \quad a_{64} = \frac{3 c_1 k \omega_1}{4 N p} + \frac{c_1 I_2 p \omega_1}{2 a_0^2 N^3}, \quad a_{71} = \frac{b_1 k \omega_1}{2 N p} + \frac{b_1 I_2 p \omega_1}{a_0^2 N^3},$$

$$a_{72} = -\frac{c_1 k \omega_1}{2 N p} + \frac{c_2 k \omega_1}{N p} - \frac{c_1 I_2 p \omega_1}{a_0^2 N^3}, \quad a_{73} = \frac{a_0 k \omega_1}{2 p} - \frac{2 I_2 p \omega_1}{a_0 N^2}, \quad a_{74} = \frac{c_2 k \omega_1}{2 N p},$$

$$a_{81} = \frac{b_2 k \omega_1}{2 N p} + \frac{3 b_2 I_2 p \omega_1}{2 a_0^2 N^3}, \quad a_{82} = -\frac{c_2 k \omega_1}{2 N p} - \frac{3 c_2 I_2 p \omega_1}{2 a_0^2 N^3}, \quad a_{83} = \frac{b_1 k \omega_1}{4 N p} + \frac{3 b_1 I_2 p \omega_1}{2 a_0^2 N^3},$$

$$a_{84} = -\frac{c_1 k \omega_1}{4 N p} - \frac{3 c_1 I_2 p \omega_1}{2 a_0^2 N^3}, \quad a_{91} = a_{92} = 0, \quad a_{93} = \frac{b_2 k \omega_1}{4 N p} + \frac{2 b_2 I_2 p \omega_1}{a_0^2 N^3},$$

$$a_{94} = -\frac{c_2 k \omega_1}{4 N p} - \frac{2 c_2 I_2 p \omega_1}{a_0^2 N^3}, \quad x_1 = l_1, \quad x_2 = m_1, \quad x_3 = l_2, \quad x_4 = m_2,$$

$$f_1 = \frac{a_1 c_1 k \omega_1}{2 p} + \frac{a_2 c_2 k \omega_1}{4 p}, \quad f_2 = \frac{a_2 c_1 k \omega_1}{4 p} + \frac{a_1 c_2 k \omega_1}{2 p} + \frac{c_1 I_2 p \omega_1}{a_0 N^2},$$

$$f_3 = -\frac{a_1 c_1 k \omega_1}{2 p} + \frac{2 c_2 I_2 p \omega_1}{a_0 N^2}, \quad f_4 = -\frac{a_2 c_1 k \omega_1}{4 p} - \frac{a_1 c_2 k \omega_1}{2 p}, \quad f_5 = -\frac{a_2 c_2 k \omega_1}{4 p},$$

$$f_6 = \frac{a_2 b_1 k \omega_1}{4 p} - \frac{a_1 b_2 k \omega_1}{2 p} + \frac{a_0 a_1 k N \omega_1}{p} - \frac{b_1 I_2 p \omega_1}{a_0 N^2}, \quad f_8 = \frac{a_2 b_1 k \omega_1}{4 p} + \frac{a_1 b_2 k \omega_1}{2 p},$$

$$f_7 = \frac{a_1 b_1 k \omega_1}{2 p} + \frac{a_0 a_2 k N \omega_1}{2 p} - \frac{2 b_2 I_2 p \omega_1}{a_0 N^2}, \quad f_9 = \frac{a_2 b_2 k \omega_1}{4 p}.$$

Appendix III

Coefficients in Equation (2-17) :

$$q0 = -0.5 (b_1 l_1 + b_2 l_2 + c_1 m_1 + c_2 m_2) + (a_0 N)^2$$

$$q1 = \frac{1}{p}\{-0.5\,(b_2\,l_1 + b_1\,l_2 + c_2\,m_1 + c_1\,m_2) - a_0\,n\,(b_1 - l_1)\}$$

$$q2 = \frac{1}{2\,p}\{-0.5\,(b_1\,l_1 - c_1\,m_1) - a_0\,N\,(b_2 - l_2)\},$$

$$q3 = \frac{1}{3\,p}\{-0.5\,(b_2\,l_1 + b_1\,l_2 - c_2\,m_1 - c_1\,m_2)\},\quad q4 = \frac{1}{4\,p}\{-0.5\,(b_2\,l_2 - c_2\,m_2)\}$$

$$p1 = \frac{1}{p}\{-0.5\,(c_2\,l_1 - c_1\,l_2 - b_2\,m_1 + b_1\,m_2) - a_0\,N\,(c_1 - m_1)\}$$

$$p_2 = \frac{1}{2\,p}\{-0.5\,(c_1\,l_1 + b_1\,m_1) - a_0\,N\,(c_2 - m_2)\}$$

$$p_3 = \frac{1}{3\,p}\{-0.5\,(c_2\,l_1 + c_1\,l_2 + b_2\,m_1 + b_1\,m_2)\},\quad p4 = \frac{1}{4\,p}\{-0.5\,(c_2\,l_2 + b_2\,m_2)\}$$

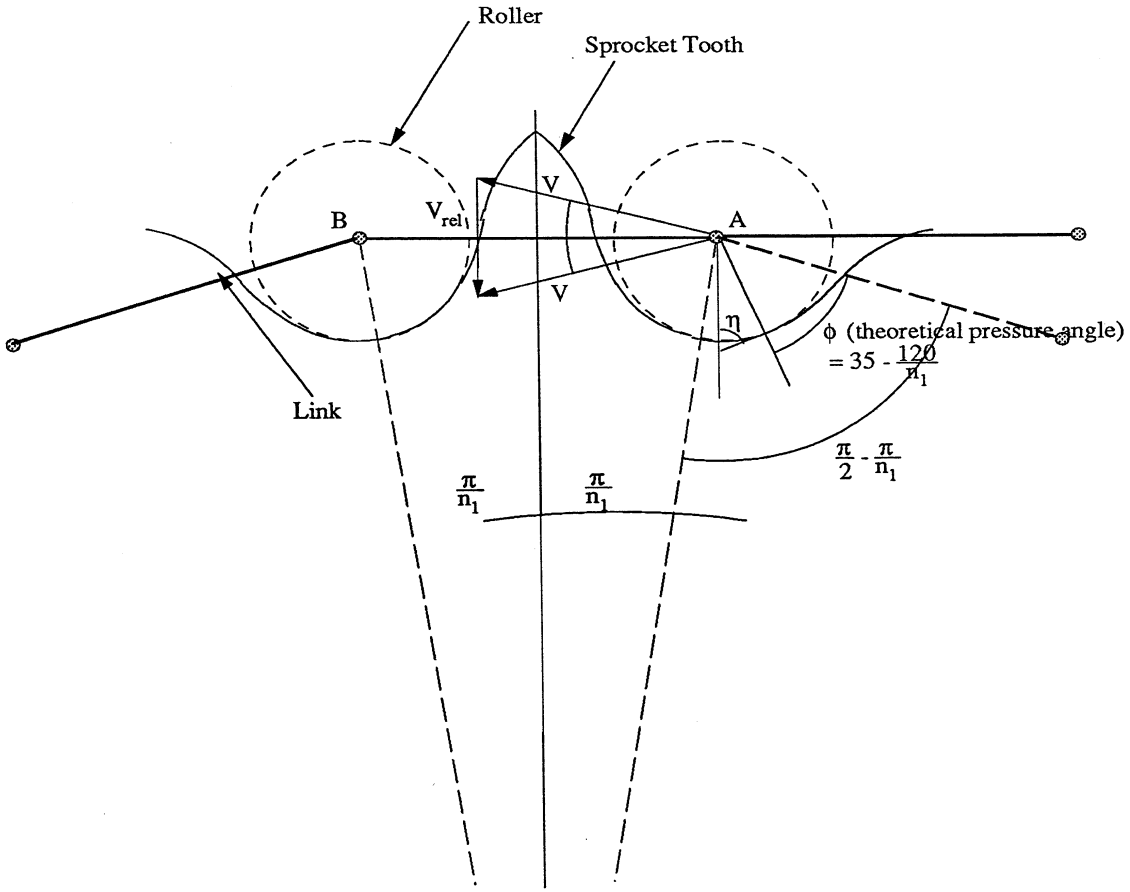

(a) Position of Rollers and Contact Angles at the Instant of Impact

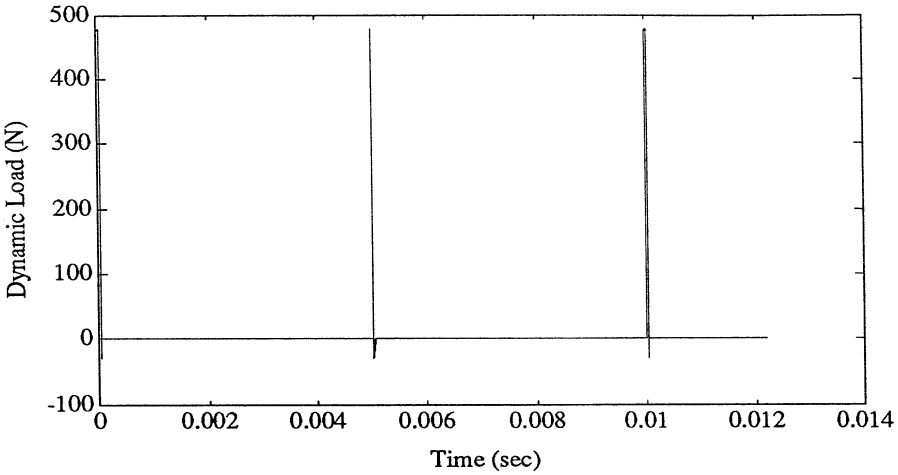

(b) Shape of Dynamic Load in Wide Time Range

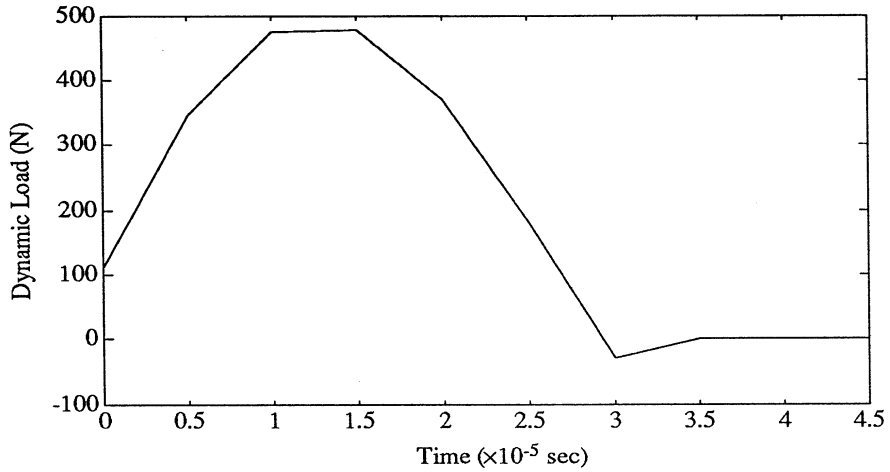

(c) Shape of Dynamic Load near Impact

Figure 1 Impact Pheonomenon Iin Roller Chain Drive

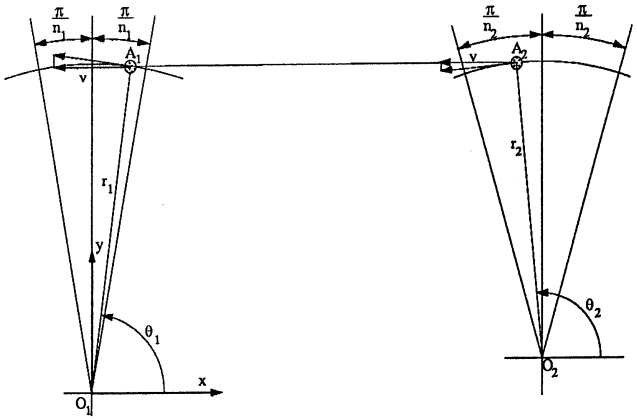

re 2 Equivalent Four-Bar Mechanism for The Calculation of Angular Velocity of Driven Sprocket

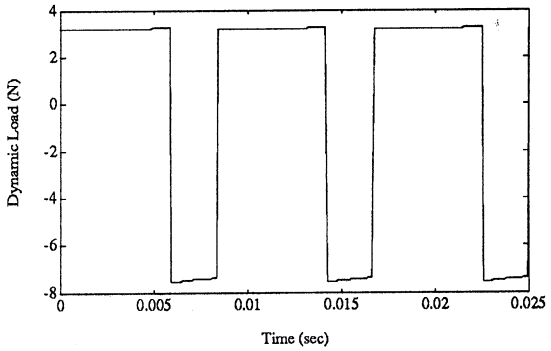

(a) case 1 : ω_1 = 300 rpm, n_1 = 24, n_2 = 24

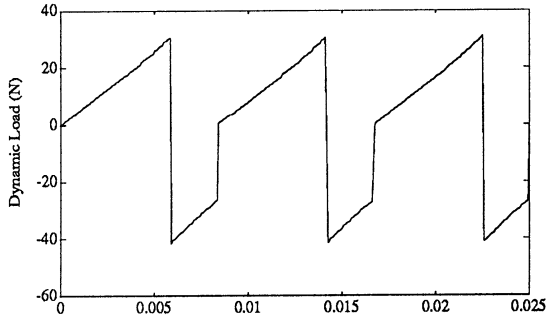

(b) case 2 : ω_1 = 300 rpm, n_1 = 24, n_2 = 15

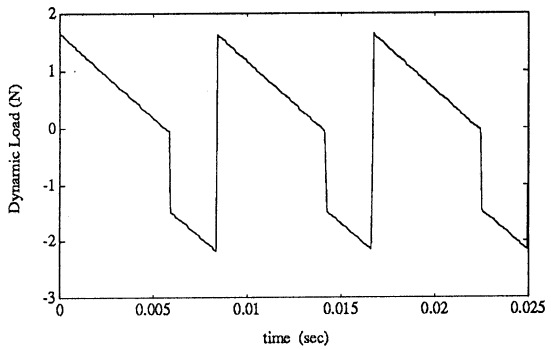

(c) case 3 : ω_1 = 300 rpm, n_1 = 24, n_2 = 40

Figure 3 Angular Velocity of Driven Sprocket and Dynamic Load Due to Polygonal Action for Rigid Chain Span

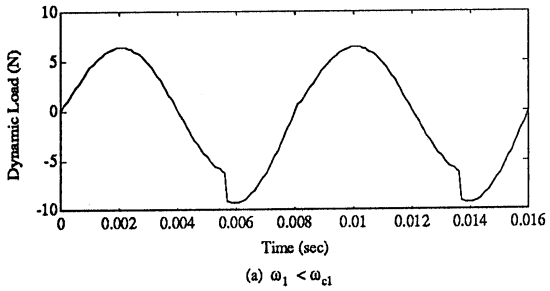

(a) $\omega_1 < \omega_{c1}$

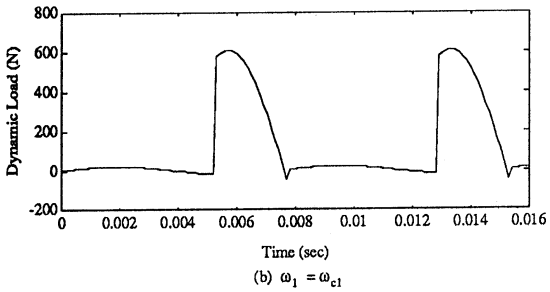

(b) $\omega_1 = \omega_{c1}$

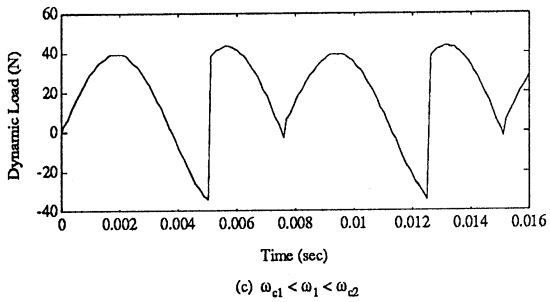

(c) $\omega_{c1} < \omega_1 < \omega_{c2}$

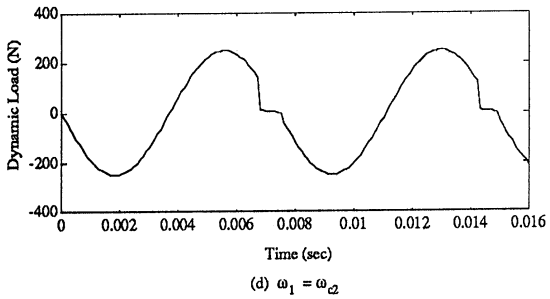

(d) $\omega_1 = \omega_{c2}$

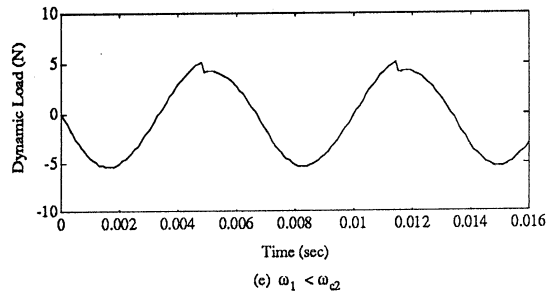

(e) $\omega_1 < \omega_{c2}$

Figure 4 Dynamic Load Due to Polygonal Action for Elastic Chain Span

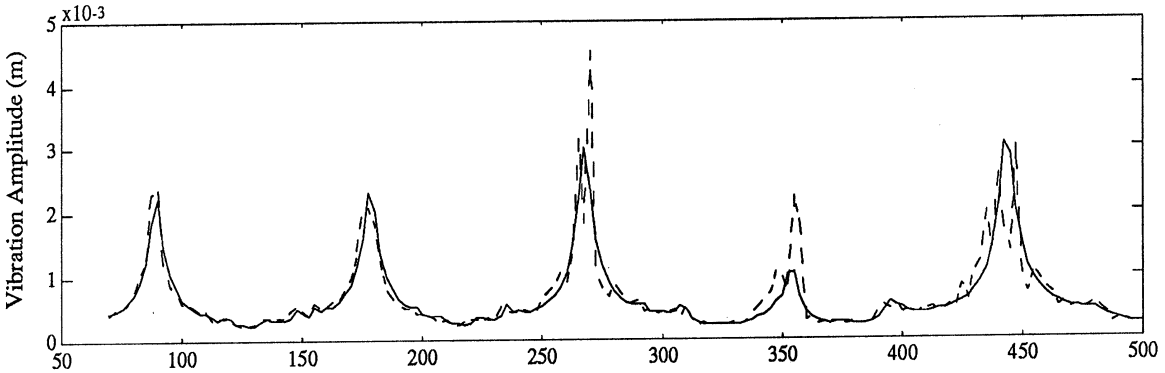

(a) center distance = 19.7 pitches

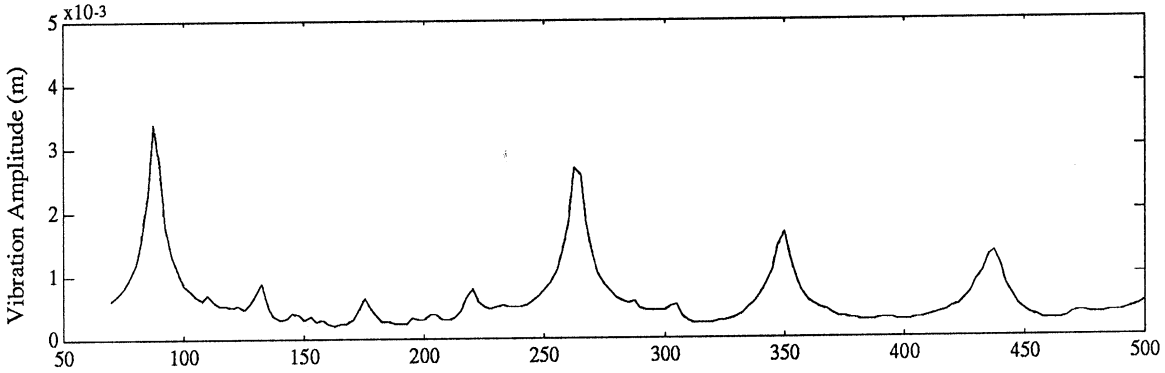

(b) center distance = 20 pitches

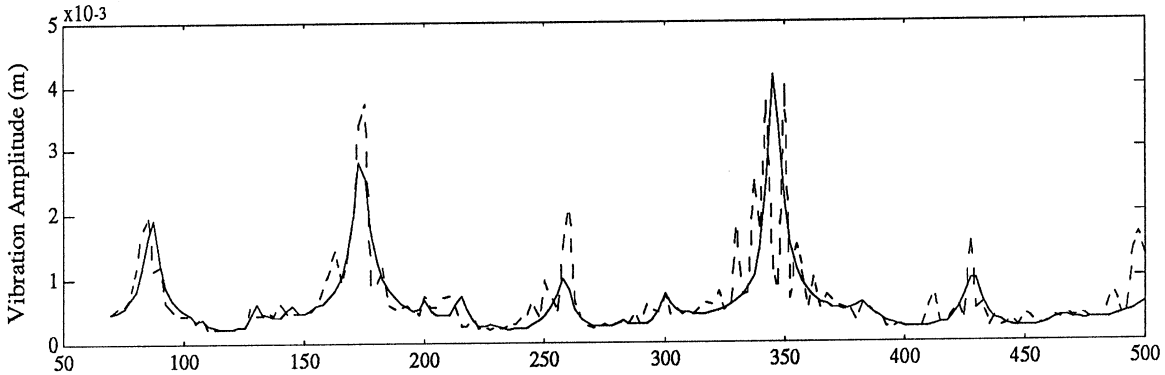

(c) center distance = 20.3 pitches

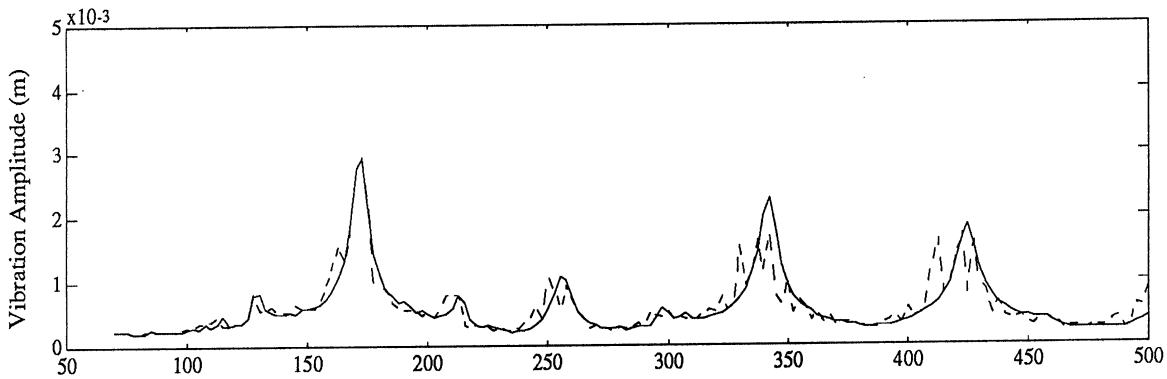

(d) center distance = 20.5 pitches

Figure 5 Effect of Periodic Length Change on Transverse Vibration
(Solid : without length change, Dashed : with length change)

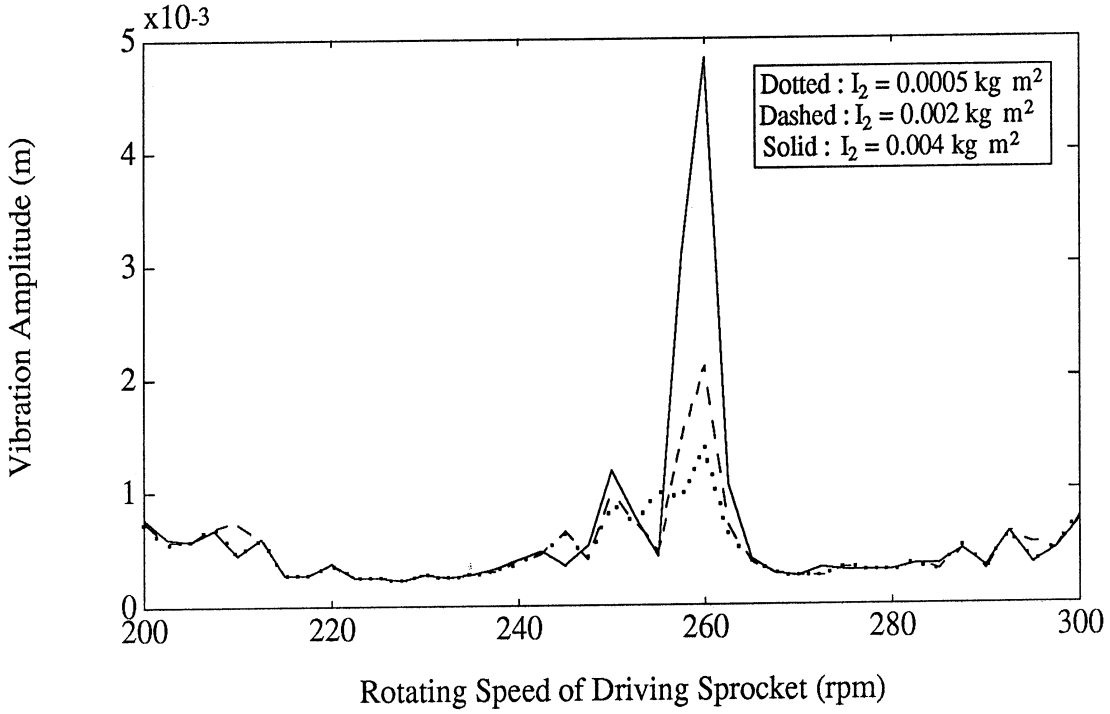

(a) Around Third Resonance

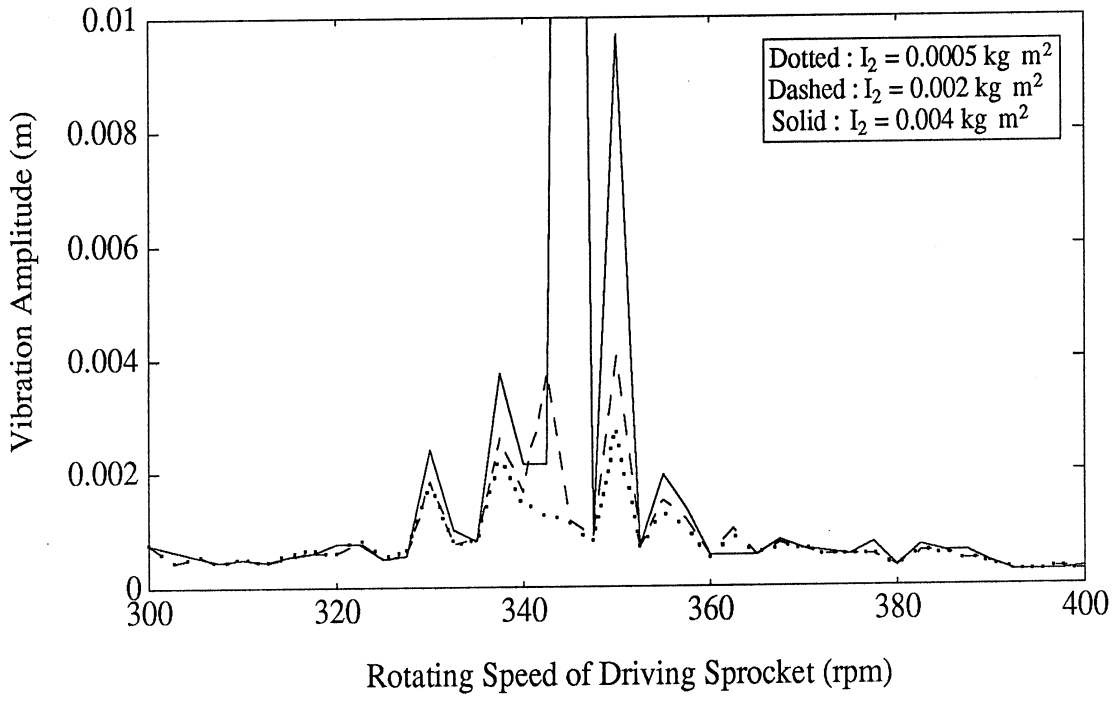

(b) Around Fourth Resonance

Figure 6 Effect of Moment of Inertia for Driven Sprocket System

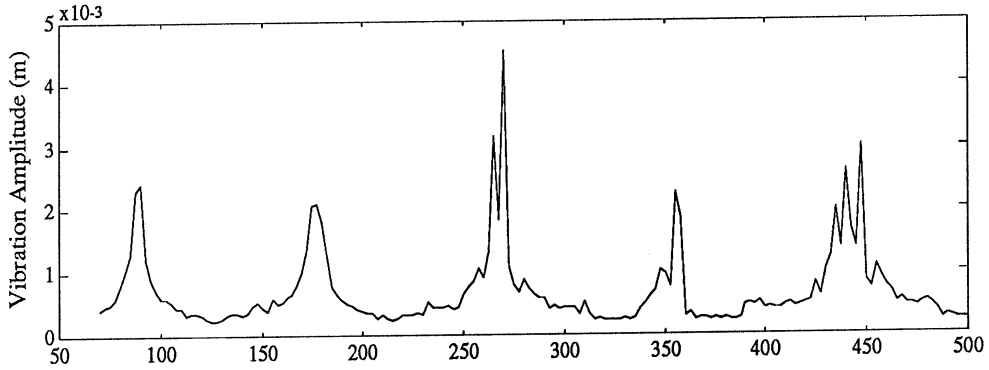

(a) $T_s = 200$ N

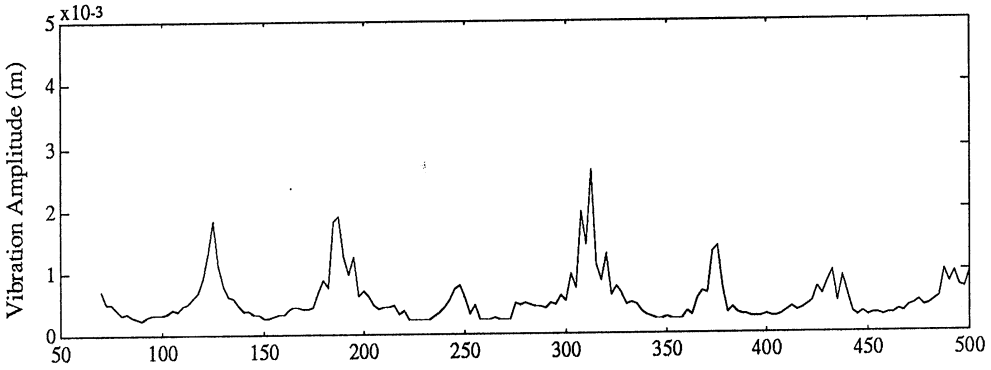

(b) $T_s = 100$ N

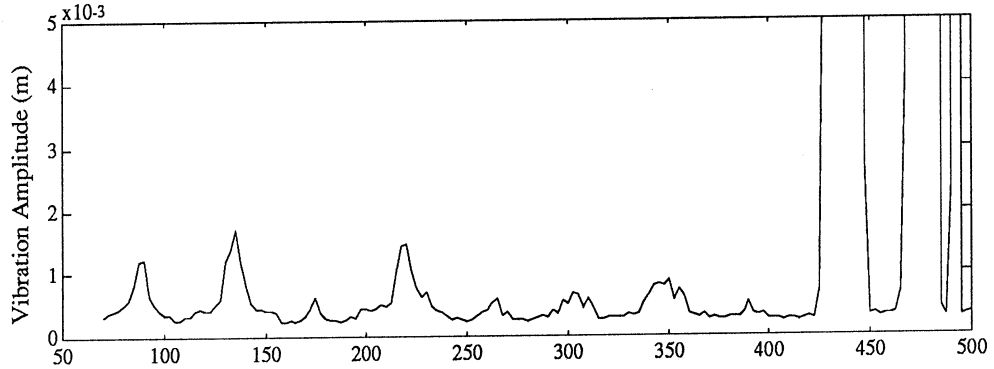

(c) $T_s = 50$ N

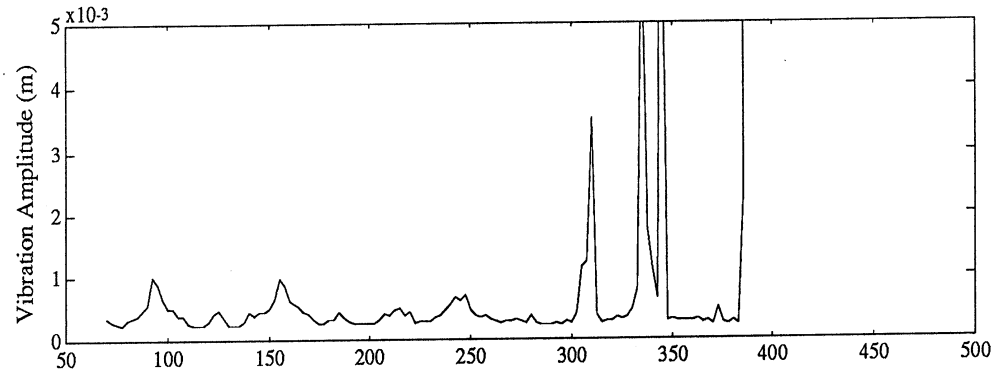

(d) $T_s = 25$ N

Figure 7 Effect of Static Tension on Transverse Vibration

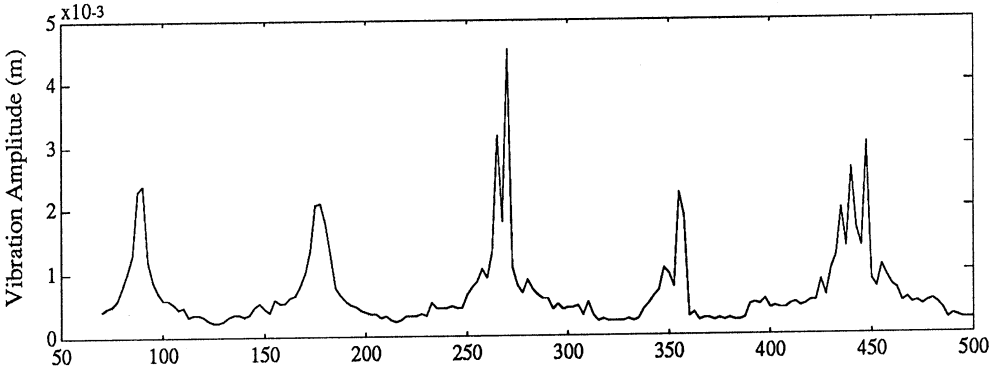

(a) without external load

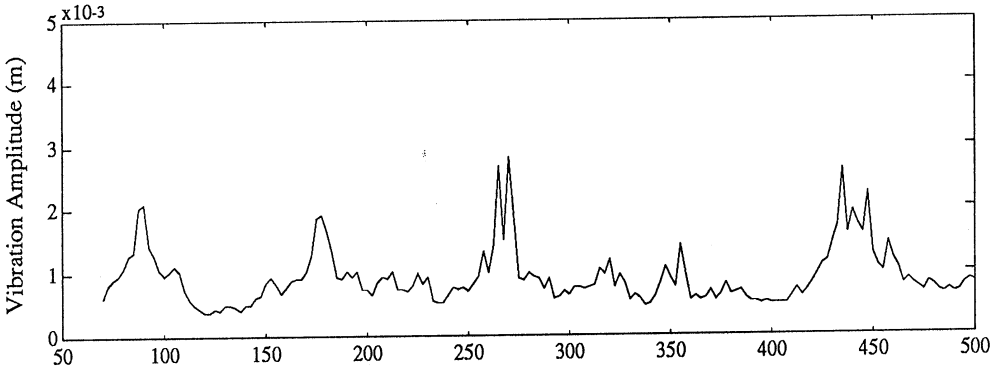

(b) $T_{ex} = 0.2\ T_s$, $\omega_{ex} = 4\ \omega_1$

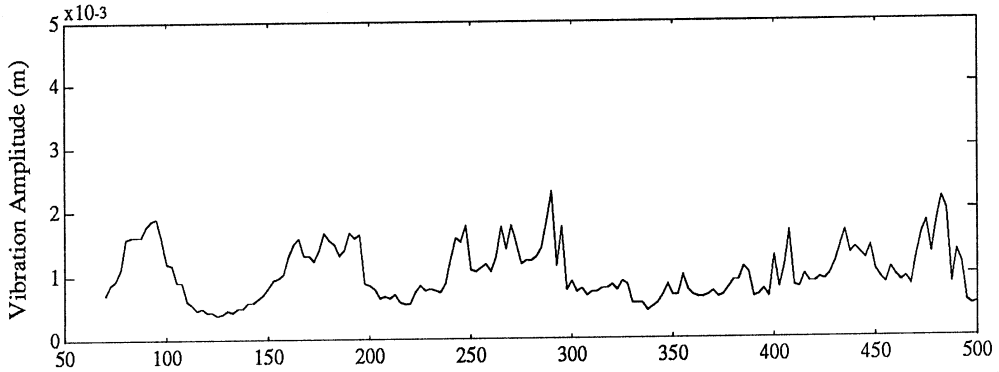

(c) $T_{ex} = 0.2\ T_s$, $\omega_{ex} = 2\omega_1$

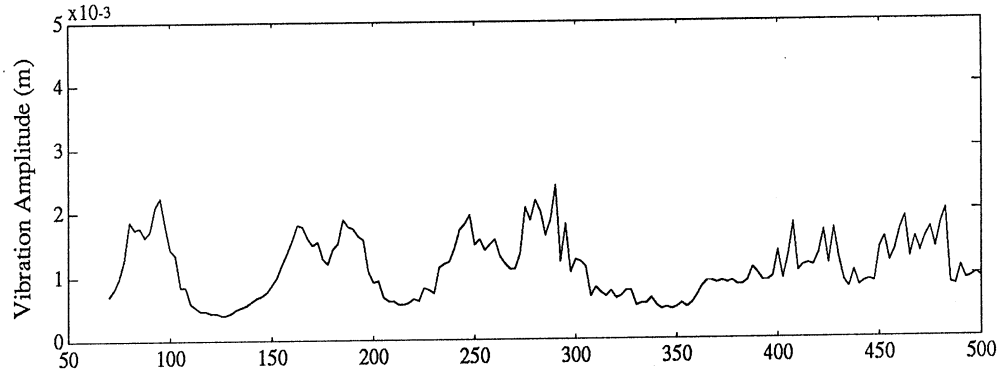

(d) $T_{ex} = 0.2\ T_s$, $\omega_{ex} = \omega_1$

Figure 8 Effect of Frequency of External Load on Transverse Vibration

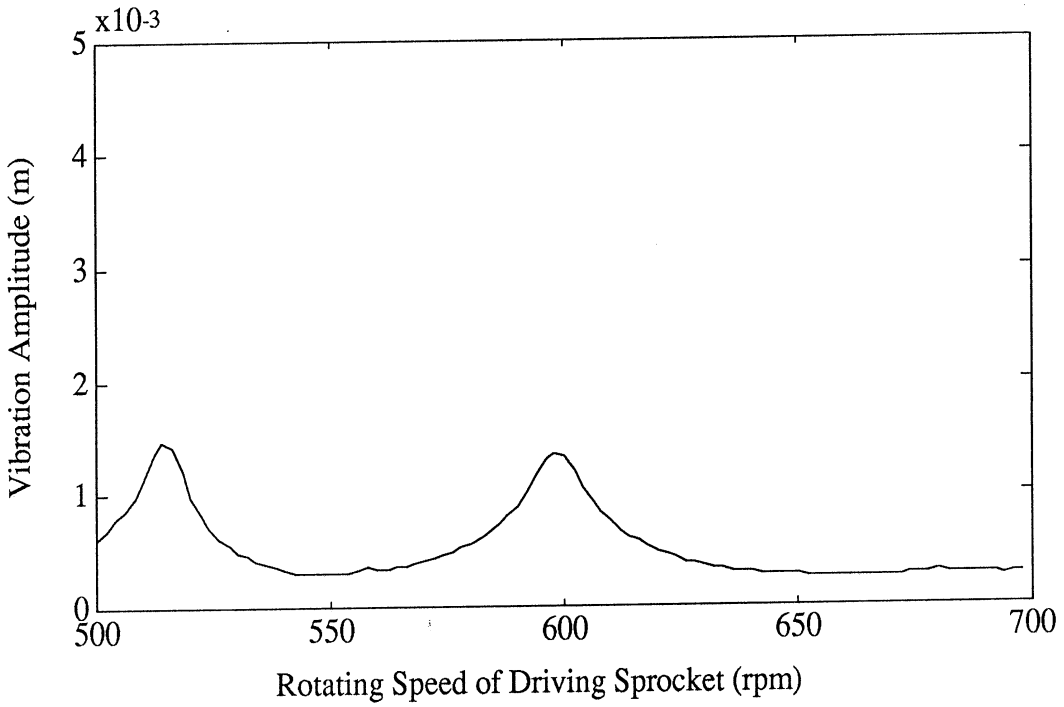

(a) No instabilities due to polygonal action in elastic chain span

($n_1 = 24$, $n_2 = 24$, $I_2 = 0.002$)

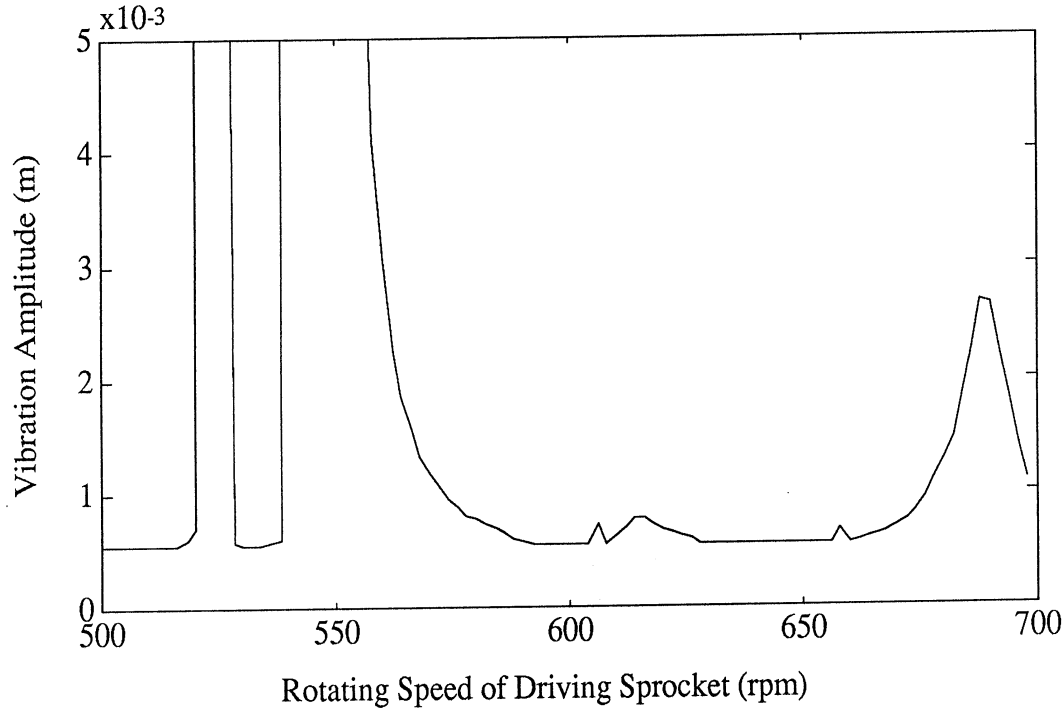

(b) Instabilities due to polygonal action in elastic chain span

($n_1 = 15$, $n_2 = 40$, $I_2 = 0.0005$)

Figure 9 Transverse Vibraion of Chain Drive at Medium Operating Speeds

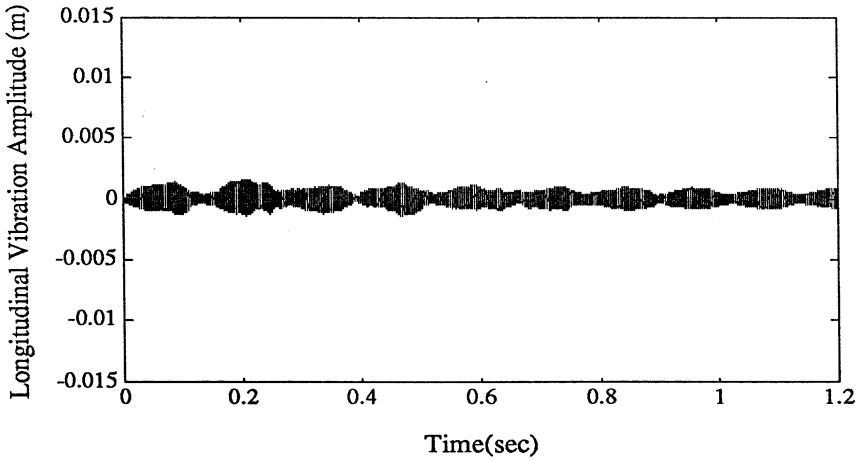

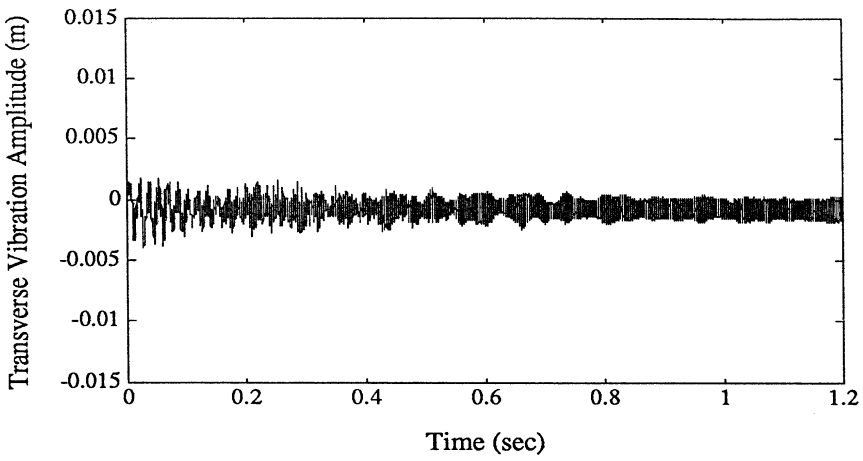

(a) Vibration Amplitudes at 1/3 Span Length Position from Driven Sprocket Near First Longitudinal Resonance

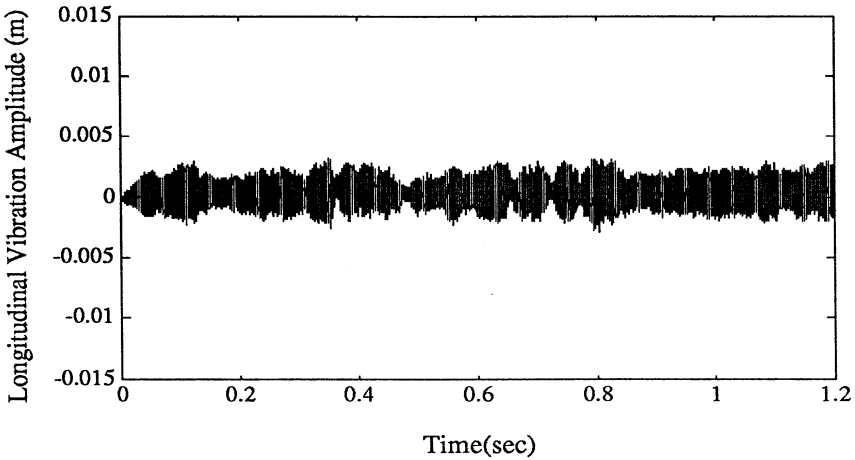

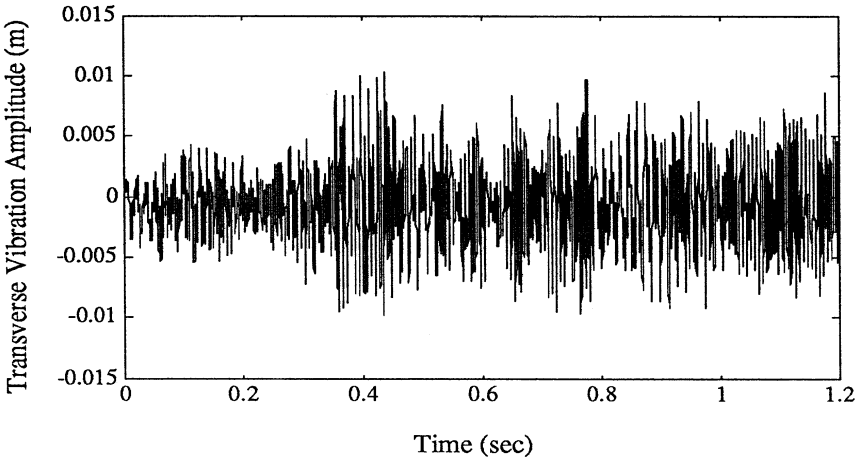

(b) Vibration Amplitudes at 1/3 Span Length Position from Driven Sprocket Near Fifth Transverse Resonance

Figure 10 Vibration Signals Changing from Transient to Steady State